IEEE Access
Multidisciplinary ⋮ Rapid Review ⋮ Open Access Journal

Received 18 September 2023, accepted 3 October 2023, date of publication 6 October 2023, date of current version 11 October 2023.

Digital Object Identifier 10.1109/ACCESS.2023.3322569

RESEARCH ARTICLE

Kinematic Calibration and Compensation of Industrial Robots Based on Extended Joint Space

WEI HE[1], PIN ZHANG[2], KAI GUO[1], (Member, IEEE), JIE SUN[1], VINOTHKUMAR SIVALINGAM[1], AND XIAOMING HUANG[3]

[1]Key Laboratory of High Efficiency and Clean Mechanical Manufacture of Ministry of Education, Department of Mechanical Engineering, Shandong University, Jinan 250061, China
[2]Aviation Key Laboratory of Science and Technology on High Performance Electromagnetic Windows, AVIC Research Institute for Special Structure of Aeronautical Composite, Jinan 250023, China
[3]Mechatronics Engineering Department, Binzhou University, Binzhou 256603, China

Corresponding author: Kai Guo (kaiguo@sdu.edu.cn)

This work was supported in part by the National Natural Science Foundation of China under Grant 51975335, Grant 52375452, and Grant 52175419; in part by the National Key Research and Development Program of China under Grant 2022YFB3206701; in part by the Key Research and Development Program of Shandong Province under Grant 2022CXGC020202; and in part by the Open Fund of Laboratory of Aerospace Servo Actuation and Transmission under Grant LASAT-2022-A01-03.

ABSTRACT The application of robots in high-precision automated machining is constrained by their limited multi-directional repeatability. In contrast, robots demonstrate superior levels of unidirectional repeatability, implying the potential for enhancing their precision. To further improve the positioning accuracy of robots, backlash error induced by rotating direction is considered, the concept of robot joint extended space is proposed, and the robot kinematic model is used to analyze the spatial similarity of robot error in the extended joint space. The dynamic Kriging method based on the optimization of basis functions is proposed to avoid overfitting of the surrogate model, and a model for estimating the robot's positioning error in the joint extended space is constructed. Based on the estimated positioning error, the proposed calibration method is finally experimentally validated by error feedforward compensation. The results indicate that after Kriging interpolation in the robot joint space and feedforward compensation, the maximum/average positioning error of the robot is improved from 1.5157 mm and 0.8562 mm before compensation to 0.3471 mm and 0.1856 mm after compensation, and then further improved to 0.1848 mm and 0.1197 mm after adopting joint expansion space and dynamic Kriging interpolation, which decreases by 46.7% and 33.5%, respectively. This method effectively compensates the multi-directional repeatability error introduced by the joint backlash and improves the robot's positioning accuracy.

INDEX TERMS Industrial robots, calibration, joint-dependent errors, error compensation.

I. INTRODUCTION

Due to their openness, dexterity, rapid reconfiguration, and low cost, industrial robots have become popular [1], [2] in recent years for assembly, welding, grinding, polishing, and loading/unloading. However, as a result of the tandem robot's open kinematic chain, their absolute positioning accuracy is typically only $\pm 1 \sim 2$ mm [3]. The robot kinematic model-based offline programming technology relies significantly on absolute positioning accuracy [4]. To successfully promote offline programming technology for high-precision manufacturing applications, the robot's absolute positioning accuracy must be enhanced with the aid of technology for accuracy compensation.

In terms of classification, there are three main strategies to improve robot accuracy [5]: error prevention, online compensation, and kinematic calibration. Error prevention is a crucial method for ensuring robot accuracy, as it eliminates or reduces errors via reasonable design, processing, assembly, and environmental control. However, the open chain structure of a tandem robot makes error prevention costly, and the cost will increase exponentially as the accuracy

The associate editor coordinating the review of this manuscript and approving it for publication was Yangmin Li.

requirement increases [6]. Online compensation demands various high-precision sensors (such as six-dimensional force sensors, laser trackers, etc.), so its widespread application is hampered by complex systems and high costs, which is presently restricted to aviation, aerospace, and other high-end manufacturing applications [7]. Kinematic calibration is the process of improving the robot accuracy by analyzing the causes of errors, establishing an error model based on the error measurement results, and adjusting to the robot's positions using the corresponding compensation method [8]. Compared to error prevention and online compensation, kinematic calibration is more economical and widely used.

Currently, robot kinematic calibration methods are divided into two categories [9]: model-based kinematic calibration and non-kinematic calibration. The model-based kinematic calibration technique identifies the robot's kinematic parameters using the least square method (LSM) [10], extended Kalman filter (EKF) [11], Levenberg-Marquardt algorithm (LM) [12], etc., after establishing the kinematic model. Finally, the error is corrected by modifying the robot controller's kinematic parameters. The Modified Denavit-Hartenberg (MD-H) model [13], the S-model [14], the complete and parametrically continuous (CPC) model [15], and the product of exponentials (POE) model [16] are typical robot modeling techniques. It is necessary to develop error models based on robot configuration and dimensions, which lack flexibility for different robot systems. Furthermore, the correction of robot kinematic parameters necessitates high open access to the controller, which severely restricts its application and diffusion.

To overcome the limitations of the model-based calibration technique, a non-kinematic calibration method that does not require a robot kinematic model is proposed [17]. The non-kinematic calibration method disregards the specific mechanism of the error source, instead treating the robot system as a "black box" and replacing the mapping relationship between the positioning error and the theoretical position or joint angle with a nonlinear model, such as a polynomial model [18] or neural network model [19]. In addition, an interpolation method based on spatial similarity of the positioning error is proposed [20]. The above non-kinematic calibration method is highly versatile and independent of robot configuration, but the robot must have excellent repeatability in multi-direction.

In fact, the unidirectional repeatability of the robot is quite high (about ±0.06 mm), while the multi-directional repeatability is poor (about ±0.15 mm) [21]. Literature [22] indicates that backlash error induced by joint rotating direction is a significant factor contributing to unidirectional repeatability, and which is much larger than the robot's unidirectional repeatability. Due to the fact that the above compensation methods are based on the robot's theoretical position, or joint spaces, they do not account for the multi-directional error caused by joint backlash. As a result, the robot's accuracy after compensation is still three to six times the unidirectional repeatability, which cannot be improved further. According to previous research, the joint backlash error can be expressed as a periodic function of the joint angle and is related to the joint's rotating direction [23]. Therefore, the robot's positioning error can be expressed as a nonlinear function of joint angle and direction.

Based on the above, the direction coefficient of robot joint is proposed, and the concept of extended joint space is developed in this article. The dynamic Kriging algorithm based on Pearson correlation coefficient (PCC) and principal component analysis (PCA) is proposed, in order to avoid overfitting of the standard Kriging algorithm when multiple input parameters exist in an extended joint space. Furthermore, a generalized pattern search (GPS) is used to establish the mapping model of the extended joint space and the positioning error, and command feedforward is employed to compensate the positioning error. The remainder of this article is organized as follows: The spatial similarity of the robot's positioning error in its extended joint space is analyzed based on the kinematic model in Section II. In Section III, the error modeling and error compensation techniques based on the dynamic Kriging algorithm are described. Experimental validation of the proposed robot calibration method is presented in Section IV. Finally, the article is summarized by a conclusion and outlook in Section V.

II. SPATIAL SIMILARITY OF POSITIONING ERRORS

A. ERROR MODELING BASED ON MD-H

According to the MD-H model definition [13], the kinematic model parameters θ_i, d_i, a_i, α_i, and β_i are the rotation angle from x_{i-1} to x_i about z_{i-1}, the distance from x_{i-1} to x_i along z_{i-1}, the distance from z_{i-1} to z_i along x_i, the angle from z_{i-1} to z_i about x_i, and the twist angle about y_i, respectively. Consequently, the homogeneous transformation matrix between two consecutive links $i-1$ and i can be written as follows:

$$T_i^{i-1} = Rot\,(z_{i-1}, \theta_i)\, Tr\,(z_{i-1}, d_i)\, Tr\,(x_i, a_i)\, Rot\,(x_i, \alpha_i)\, Rot\,(y_i, \beta_i) \tag{1}$$

where $Rot\,(j, \bullet)$ is the rotation matrix about j, and $Tr\,(j, \bullet)$ is the translation matrix along j. If $\Delta\theta_i$, Δd_i, Δa_i, $\Delta\alpha_i$ and $\Delta\beta_i$ represent the errors of the kinematic parameters for the i-th joint, then the actual transformation matrix of the n-DOF robot from the tool center point (TCP) to the base frame can be expressed as:

$$\tilde{T} = \prod_{i=1}^{n} \tilde{T}_i^{i-1} = \prod_{i=1}^{n} \left(T_i^{i-1} + \delta T_i^{i-1} \right) \tag{2}$$

where δT_i^{i-1} is the error transformation matrix. Due to the error of each kinematic parameter is tiny, it can be approximated as a simple linear equation:

$$\delta T_i^{i-1} = \frac{\partial T_i^{i-1}}{\partial \theta_i} \Delta\theta_i + \frac{\partial T_i^{i-1}}{\partial d_i} \Delta d_i + \frac{\partial T_i^{i-1}}{\partial a_i} \Delta a_i$$

$$+\frac{\partial T_i^{i-1}}{\partial \alpha_i}\Delta\alpha_i+\frac{\partial T_i^{i-1}}{\partial \beta_i}\Delta\beta_i \tag{3}$$

According to (2) and (3), ignoring the higher order terms, the error between the actual and theoretical position can be calculated as follows:

$$\Delta P=\sum_{i=1}^{n}\left(\frac{\partial T}{\partial \theta_i}\Delta\theta_i+\frac{\partial T}{\partial d_i}\Delta d_i+\frac{\partial T}{\partial a_i}\Delta a_i+\frac{\partial T}{\partial \alpha_i}\Delta\alpha_i+\frac{\partial T}{\partial \beta_i}\Delta\beta_i\right) \tag{4}$$

where $\frac{\partial T}{\partial \bullet}=T_2^1T_3^2\cdots\frac{\partial T_i^{i-1}}{\partial \bullet}\cdots T_6^5$, $\bullet$ denotes the robot kinematic parameters, i.e., θ_i, d_i, a_i, α_i, and β_i.

B. SPATIAL SIMILARITY OF POSITIONING ERRORS IN EXTENDED JOINT SPACE

From (1), it is clear that the kinematic parameters, i.e., link offset d_i, link length a_i, link twist α_i, and twist angle β_i, of the MD-H model for the tandem rotary joint robot are all constants, with only the joint angle θ_i being a free variable. Therefore, the positioning errors caused by the kinematic parameter errors can be viewed as deterministic functions about the joint angle, reflecting in part the character of the robot, its unidirectional repeatability is exceptionally precise.

Due to there exists a gap between the meshing gears, the reverse motion of the joint will lead to the backlash [24], and the actual joint angle deviates from the theoretical joint angle for the same joint angle command. It is demonstrated that the robot joint angle error is a function of the motion direction and the theoretical joint angle, and is typically assumed to be a constant error, i.e., of the same magnitude in forward and reverse directions to the specified angle [25], so that the actual joint angle can be expressed as:

$$\tilde{\theta}_i=\theta_i+\lambda_i b_i(\theta_i) \tag{5}$$

with

$$\lambda_i=\begin{cases}1, \textit{forward motion}\\ -1, \textit{backward motion}\end{cases}$$

where λ_i, $b_i(\theta_i)$ are the directional coefficient and the backlash error corresponding to the joint angle θ_i, respectively. It is evident from the preceding analysis that the joint backlash influences the TCP position by affecting the actual joint angle of the robot. When the theoretical joint angle and direction are comparable, the corresponding positioning errors are similar. Thus, this article establishes an extended joint space $[\theta_1,\cdots,\theta_n,\lambda_1,\cdots,\lambda_n]$ by introducing the directional coefficient of the joint angle in the joint space of a n-degree-of-freedom serial robot in order to account for the effect of rotating direction on robot accuracy, and enhance its multi-directional positioning accuracy.

III. ERROR MODELING AND COMPENSATION

A. ERROR MODELING IN EXTENDED JOINT SPACE

In order to estimate the positioning error at any point in the robot workspace, the standard Kriging method [26] from spatial statistics is introduced to establish the mapping relationship between joint angle and directional coefficient and positioning error in the extended joint space using limited measured data.

According to Kriging interpolation theory, given a set of m samples in extended joint space, $S=[s_1,\cdots,s_m]^T$ with $s_i=[\theta_{i1},\cdots,\theta_{in},\lambda_{i1},\cdots,\lambda_{in}]\in R^{2n}$,and m responses $\Delta=[\delta_1,\ldots,\delta_m]^T$ with $\delta_i\in R^q$. S, Δ satisfy the normalization conditions, i.e., $\mu(S_{:,j})=0$, $\sigma(S_{:,j})=1$, $j=1,\cdots,2n$, $\mu(\Delta_{:,k})=0$, $\sigma(\Delta_{:,k})=1$, $k=1,\cdots,q$. Then, the k-direction positioning error δ_k can be expressed as:

$$\hat{\delta}_k(s)=E(\boldsymbol{\beta}_{:,k},s)+z_k(s) \tag{6}$$

In (1), the positioning error is composed of both mean and stochastic errors, with the mean error $E(\boldsymbol{\beta}_{:,k},\mathbf{s})=\mathbf{f}^T(\mathbf{s})\,\boldsymbol{\beta}_{:,k}=\sum_{i=1}^{p}f_i\beta_{i,k}$ is a regression model constructed by user-selected basis functions f_i. The basis functions f_i are usually in simple polynomial form, $\beta_{i,k}$ is the coefficient of the i-th basis function. And $z_k(s)$ is the stochastic error with a mean of 0. Its covariance between the s_i and s_j sample points can be expressed as:

$$Cov\left(z_k(s_i),z_k(s_j)\right)=\sigma_k{}^2\tilde{R}_k\left(\boldsymbol{\xi},s_i,s_j\right) \tag{7}$$

where $\sigma_k{}^2$ is the process variance in the k-direction and $\tilde{R}_k$ is the spatial correlation model with parameter $\boldsymbol{\xi}$. Typically, the correlation model in engineering problems is given the following Gaussian form:

$$\tilde{R}_k\left(\boldsymbol{\xi},s_i,s_j\right)=\exp\left(-\sum_{k=1}^{2n}\xi_k\left|s_{i,k}-s_{j,k}\right|^2\right) \tag{8}$$

To facilitate analysis, assuming $q=1$, i.e., $\boldsymbol{\beta}=\boldsymbol{\beta}_{:,k}$, $\Delta=\Delta_{:,k}$, consider the linear predictor:

$$\hat{\delta}(s)=c^T\Delta \tag{9}$$

where c is the weight coefficient vector for linear interpolation. Therefore, the best linear unbiased estimate of δ is:

$$\hat{\delta}(s)=f^T(s)\hat{\boldsymbol{\beta}}+r^T(s)R^{-1}(\Delta-F\hat{\boldsymbol{\beta}}) \tag{10}$$

with

$$r(s)=\left[\tilde{R}\left(\boldsymbol{\xi},s,s_1\right),\tilde{R}\left(\boldsymbol{\xi},s,s_2\right),\cdots,\tilde{R}\left(\boldsymbol{\xi},s,s_m\right)\right]^T$$

$$R=\begin{bmatrix}\tilde{R}\left(\boldsymbol{\xi},s_1,s_1\right)&\cdots&\tilde{R}\left(\boldsymbol{\xi},s_1,s_m\right)\\ \vdots&\ddots&\vdots\\ \tilde{R}\left(\boldsymbol{\xi},s_m,s_1\right)&\cdots&\tilde{R}\left(\boldsymbol{\xi},s_m,s_m\right)\end{bmatrix}$$

$$f(s)=\left[f_1(s),f_2(s),\cdots,f_p(s)\right]^T$$

$$F=\left[f_1(s),f_2(s),\cdots,f_m(s)\right]^T$$

In (11), the least squares estimate of $\boldsymbol{\beta}$ can be expressed as:

$$\hat{\boldsymbol{\beta}}=\left(F^TR^{-1}F\right)^{-1}F^TR^{-1}\Delta \tag{11}$$

The prediction variance of the target point s can then be expressed as:

$$\varphi(s) = \hat{\sigma}^2 \left[1 - r^T(s) R^{-1} r(s) + \left(F^T R^{-1} r(s) - f(s) \right)^T \left(F^T R^{-1} F \right)^{-1} \left(F^T R^{-1} r(s) - f(s) \right) \right] \tag{12}$$

where $\hat{\sigma}^2$ is an estimate of the process variance σ^2 and the maximum likelihood estimate of σ^2 is given as:

$$\hat{\sigma}^2 = \frac{1}{m} (\Delta - F\hat{\beta})^T R^{-1} (\Delta - F\hat{\beta}) \tag{13}$$

It can be seen from (11) and (13) that $\hat{\beta}$ and $\hat{\sigma}^2$ are dependent on the matrix R. After determining the form of the regression model and the correlation model, the matrix R is dependent on ξ, so the modeling process can be translated into the optimization of the correlation parameter ξ. If $\hat{\xi}$ is the estimate of ξ with the maximum likelihood estimator, then $\hat{\xi}$ can be expressed as:

$$\begin{cases} Minmize : \psi(\xi) = |R(\xi)|^{\frac{1}{m}} \sigma(\xi)^2 \\ Subjectto : \xi(i) \geq 0 \end{cases} \tag{14}$$

B. DYNAMIC KRIGING METHOD BASED ON BASIS FUNCTION SELECTION

Assume that the set of candidate basis functions is made up of polynomials and that the elements of the set are products of extended joint space parameters $[\theta_1, \cdots, \theta_n, \lambda_1, \cdots, \lambda_n]$ in the form:

$$f = \left[1, \theta_1, \cdots, \lambda_n, \theta_1^2, \cdots, \lambda_n^2, \cdots, \theta_1^\eta, \cdots, \lambda_n^\eta \right]^T_{1 \times n_1} \tag{15}$$

where η and $n_1 = C^{\eta}_{2n+\eta}$ are the highest order and the number of candidate basis function elements, respectively. In the process of constructing the surrogate model for the standard Kriging model, the form of the basis function of the regression model E in (6) is fixed, and the higher order terms in the polynomial are typically regarded to predict the nonlinear deterministic error.

Martin and Simpson [27] noted, however, that for highly nonlinear problems, increasing the order of the basis function may not enhance the accuracy of the surrogate model. To improve the model's fitting accuracy, a dynamic Kriging approach was proposed [28], in which basis functions were chosen from the candidate basis functions using a genetic algorithm. However, with the purpose of improving operational efficiency, the correlation parameter ξ are fixed to constant values during the optimization process, which reduces the accuracy of the surrogate model to some extent. Meanwhile, the modified Hooke Jeeves (HJ) algorithm is employed for optimization, it prioritizes solution efficiency but, due to multiple input parameters in the expanded joint space and high nonlinearity, can only find the local optimum. However, accurately solving the optimal solution of (14) is necessary to increase the accuracy of the surrogate model [29]. In order to improve the operational efficiency and accuracy of the surrogate model, this paper proposes a basis function selection and fusion method based on PCC and PCA, and uses the GPS method instead of the HJ algorithm to find the optimal correlation parameters of the model accurately.

1) BASIS FUNCTION SELECTION AND FUSION

The PCC is a straightforward and effective method for determining the linear relationship [30] between two variables in the higher-order Kriging models, making it an ideal technique for choosing basis functions. For a test involving m samples, the correlation between the i-th candidate basis function f_i and the response δ can be expressed as follows:

$$\rho_{f_i,\delta} = \frac{cov(f_i, \delta)}{\sqrt{var(f_i)\, var(\delta)}} \tag{16}$$

with

$$cov(f_i, \delta) = \sum_{j=1}^{m} (f_i(s_j) - \bar{f}_i)^T (\delta_j - \bar{\delta})$$

$$var(f_i) = \sum_{j=1}^{m} (f_i(s_j) - \bar{f}_i)^T (f(s_j) - \bar{f}_i)$$

$$var(\delta) = \sum_{j=1}^{m} (\delta_j - \bar{\delta})^T (\delta_j - \bar{\delta})$$

where $cov(\bullet, \bullet)$ and $var(\bullet)$ are the covariance and variance of the variables, and $\bar{f}_i$ and $\bar{\delta}$ are the means of f_i and δ, respectively. The stronger the correlation, the closer the correlation coefficient is to 1 (-1), and the weaker the correlation, the closer the correlation coefficient is to 0. To avoid the overfitting caused by a too-large set of basis functions, the basis functions are ranked according to their correlation, and the n_2 basis functions with correlation values greater than a threshold T are selected to form the set of initial basis functions.

The set of initial basis functions can be viewed as a high-dimensional multivariate matrix formed by the extended joint space. Due to the curse of dimensionality and the high correlation between basis functions, it is not appropriate to input the above matrix into the Kriging model without dimensionality reduction. PCA provides information on the most significant variables, thereby describing the entire dataset and enabling data reduction with minimal loss of original data [31]. That is, few unrelated variables are used to express the original information, which simplifies the information and improves the fitting efficiency and accuracy of the error model. Let the set of n_2-dimensional initial basis functions be denoted by $u = [u_1, u_2, \cdots, u_{n_2}]^T$. To avoid the incomparability of basis functions due to the difference in dimension, the z-score method is first used to normalize, and then the covariance matrix of U is denoted as follows:

$$cov(U) = E\{[U - E(U)][U - E(U)]^T\} \tag{17}$$

with

$$U = [u(s_1), u(s_2), \cdots, u(s_m)]^T$$

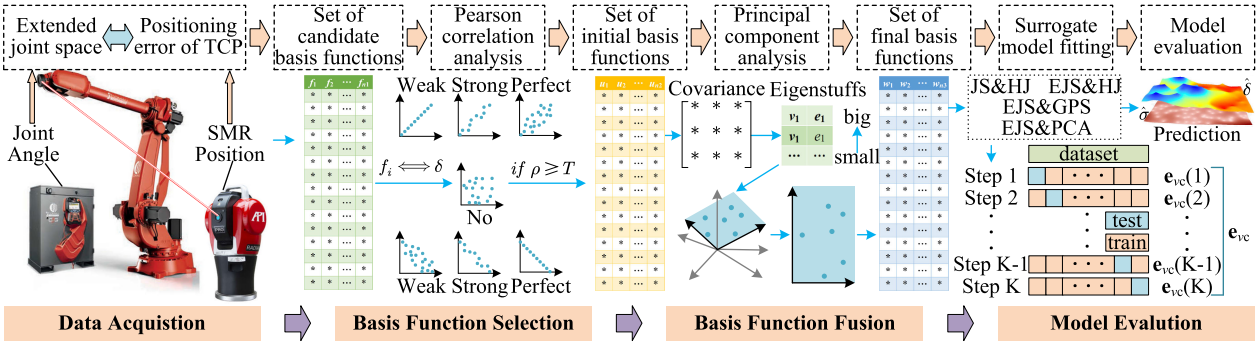

FIGURE 1. Schematic of the optimization process for the dynamic Kriging algorithm.

The eigenvalues of (17) are computed and arranged in descending order: $v_1 \geq v_2 \geq \cdots \geq v_{n_2}$; the corresponding orthogonal normalized eigenvectors are $e_1, e_2, \cdots, e_{n_2}$; the i-th modified basis function can then be expressed as:

$$w_i = u^T e_i \tag{18}$$

with

$$e_i = \left[e_{i,1}\ e_{i,2}\ \cdots\ e_{i,n_2} \right]^T$$

In practical, the principle of selection is the proportion of the first n_3 ($n_3 \leq n_2$) modified basis functions with a cumulative contribution of 99%, as shown below:

$$\gamma_{n_3} = \sum_{i=1}^{n_3} v_i / \sum_{i=1}^{n_2} v_i \tag{19}$$

Then the set of final basis functions can be expressed as:

$$w = \left[w_1, w_2, \cdots, w_{n_3} \right]^T \tag{20}$$

2) CROSS-VALIDATION METHOD

The GPS algorithm is used to find an accurate optimum for the correlation parameter ξ in order to build the Kriging surrogate model. K-fold cross-validation is then used to quantitatively compare the spatial interpolation accuracy of the surrogate models fitted by different sets of basis functions [32]. In detail, the data set $\{S, \Delta\}$ containing m data points is divided into K subsets $\{S_1, \Delta_1\}, \{S_2, \Delta_2\}, \ldots, \{S_K, \Delta_K\}$, from which one subset is randomly selected as the testing set and the remaining subsets are used as the model's training data. The procedure iterates K times until all subsets have been used as validation data sets once and a total of K validation results have been acquired. The error vector of cross-validation can then be expressed as:

$$e_{cv}(i) = \Delta_i - \hat{\Delta}(S_i)\ (i = 1, \ldots, K) \tag{21}$$

Figure 1 depicts a summary of the proposed dynamic Kriging algorithm. Firstly, the acquired robot joint angle and SMR position sets were converted into the corresponding extended joint space and TCP positioning error sets. Then, PCC was used to analyze the correlation between the candidate basis functions and positioning errors, and the basis functions with the highest correlation were chosen for the set of initial basis functions. Again, PCA was employed to reduce the dimensionality of the set of initial basis functions, and the modified basis functions with a cumulative contribution rate of 99% were chosen as the set of final basis functions. Finally, the error estimation models were established using different Kriging methods, and their accuracy was compared using K-fold cross-validation.

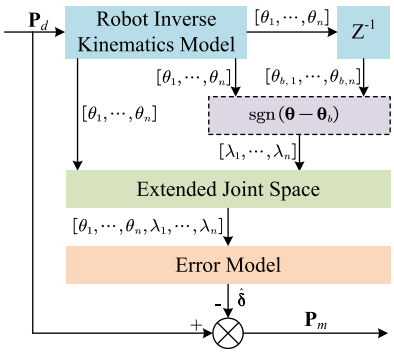

FIGURE 2. Positioning error compensation process.

C. FEEDFORWARD ERROR COMPENSATION METHOD

As shown in Figure 2, first, the theoretical joint angle is calculated. Then, the extended joint angle $[\theta_1, \cdots, \theta_n, \lambda_1, \cdots, \lambda_n]$ is determined by comparing the joint angle θ with the previous joint angle θ_b. Using the error model fitted in Section III-B and the extended joint angle of the target position P_d, the estimated positioning error is calculated. According to the spatial similarity of positioning errors, the TCP positioning errors corresponding to two sets of adjacent joint angles are comparable. So the actual position of the corrected position P_m can therefore be regarded as the target position P_d:

$$P_m = P_d - \hat{\boldsymbol{\delta}} \tag{22}$$

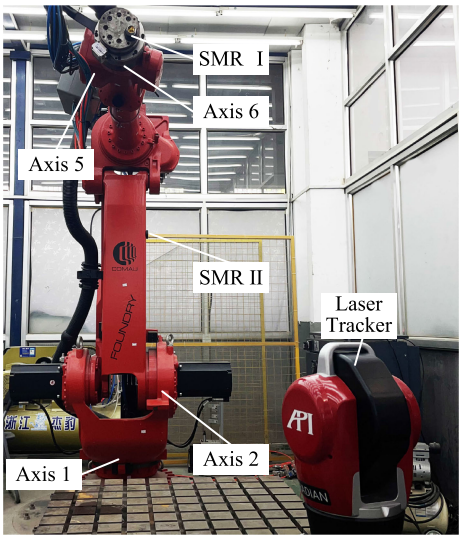

FIGURE 3. Experimental setup.

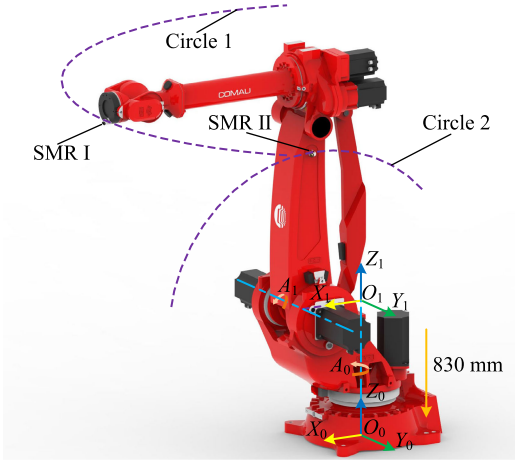

FIGURE 4. Identification the base frame.

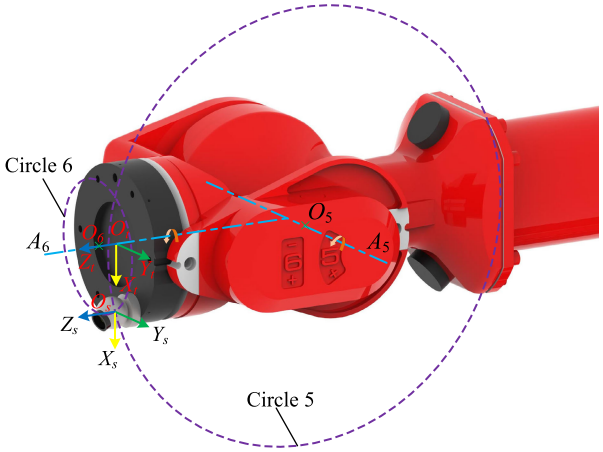

FIGURE 5. Identification the SMR offset relative to TCP.

IV. EXPERIMENTS AND RESULTS

As is shown in Figure 3, experiments are carried out on a COMAU SMART5 NJ 220 industrial robot, which has a repeatability of ±0.075 mm. API's Radian Core laser tracker, with a maximum permissible error of 15μm+5μm/m for distance, is used to measure the TCP position. In the experiment, the distance between the laser tracker and the spherical mounted retroreflector (SMR) is less than 5 m. The proposed dynamic Kriging is utilized to fit the TCP positioning error, and the error is compensated by the feedforward compensation method.

A. ROBOT FRAME IDENTIFICATION

1) BASE FRAME IDENTIFICATION

To measure the positioning error of the TCP, the base frame is constructed using Polyworks, a spatial analyzer software developed by InnovMetric, in coordination with the API laser tracker. As shown in Figure 4, the transitional frame, $O_1X_1Y_1Z_1$, is created using the circle-point-analysis (CPA) method [33], [34], and the base frame, $O_0X_0Y_0Z_0$, is obtained by translating 830 mm along the negative direction of the Z_1 of the transitional frame. The detailed procedure is as follows:

1) The SMR I is mounted on the robot end flange, rotated axis 1 as far as possible, and a set of SMR I positions measured by a laser tracker is used to fit circle 1. Fixed SMR II to robot linkage 2, axis 2 is then rotated as much as possible while the position of SMR II is again measured, and fit circle 2 in the same way.
2) The normal A_0 of the circle 1 is designated as the Z_1. The common perpendicular line of normals A_0 and A_1 is designated as the X_1, and the frame $O_1X_1Y_1Z_1$ is defined using the right-hand rule.
3) The robot's base frame, $O_0X_0Y_0Z_0$, is obtained by translating the transitional frame, $O_1X_1Y_1Z_1$, along the negative direction of its Z_1 by the nominal offset 830 mm.

2) SMR OFFSET IDENTIFICATION

Typically, offline programming software generates machining trajectories with respect to the TCP, and there is an offset between the SMR and TCP so as not to influence the machining process, as depicted in Figure 5. Therefore, in order to precisely determine the TCP positioning errors, the offset of SMR relative to TCP must be precisely estimated. Again, the CPA method is used to determine the SMR offset by rotating joints 5 and 6, as described below:

1) The SMR is mounted to the robot's end flange, and the beginning position (A6 at 0°) is recorded as O_s. Then, the SMR position is measured while the axis A_6 is rotated through 360°, and the circle 6 is fitted to the measurement data. Again, the SMR position is remeasured while the axis 5 is rotated as far as feasible, and circle 5 is fitted to the data.
2) The normal A_6 of the circle 6 is defined as the Z_t, the common perpendicular line of the Z_t and the

TABLE 1. Range of motion for robot each joint axis.

Axis	Constraint range (°)	Axis	Constraint range (°)
A1	(-20,20)	A4	(-15,15)
A2	(-30,30)	A5	(-15,15)
A3	(-120,80)	A6	(-15,15)

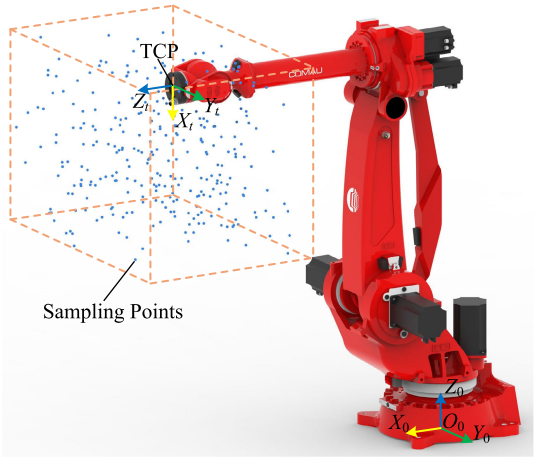

FIGURE 6. The 300 random TCP positions.

normal A_5 of the circle 5 is defined as the X_t, and the Y_t is determined by the right-hand rule. So, the rotation matrix R_t from the laser tracker to the TCP is $[X_t, Y_t, Z_t]$. The TCP origin in the laser tracker is then: $O_t = O_6 - (d - d_6) \cdot Z_t$, where O_5 and O_6 are the circle center coordinates of circles 5 and 6, respectively, d is the projection length of vector O_5O_6 on the Z_t, and d_6 is the nominal length of robot linkage 6.

3) Based on the TCP origin O_t and the transition matrix R_t, it is possible to derive the coordinates of O_s in the TCP frame, i.e., the SMR offset: $P_{\text{SMR}} = R_t^{-1}(O_s - O_t)$.

B. DYNAMIC KRIGING ALGORITHM VALIDATION

1) BASIS FUNCTION SELECTION

After the base frame and the SMR offset have been determined, the SMR positions in the laser tracker frame are transformed into TCP positions in the base frame. As shown in Figure 6, 300 random target points were generated using Latin hypercube sampling (LHS) in the robot workspace, with joint angle range as the constraint (see Table 1). The actual position of TCP is determined using a laser tracker, and the positioning error of each point along the X_0, Y_0, and Z_0 axes is identified.

Figure 7 shows the Pearson correlation between the TCP positioning error and the second-order polynomial basis functions of the extended joint space parameters. As observed, the base functions related to the directional coefficient are ranked third, second, and fourth, respectively, for the X_0, Y_0, and Z_0 axes, indicating that the joint backlash error has a significant impact on the robot's positioning accuracy. Moreover, the correlation ranking differences of

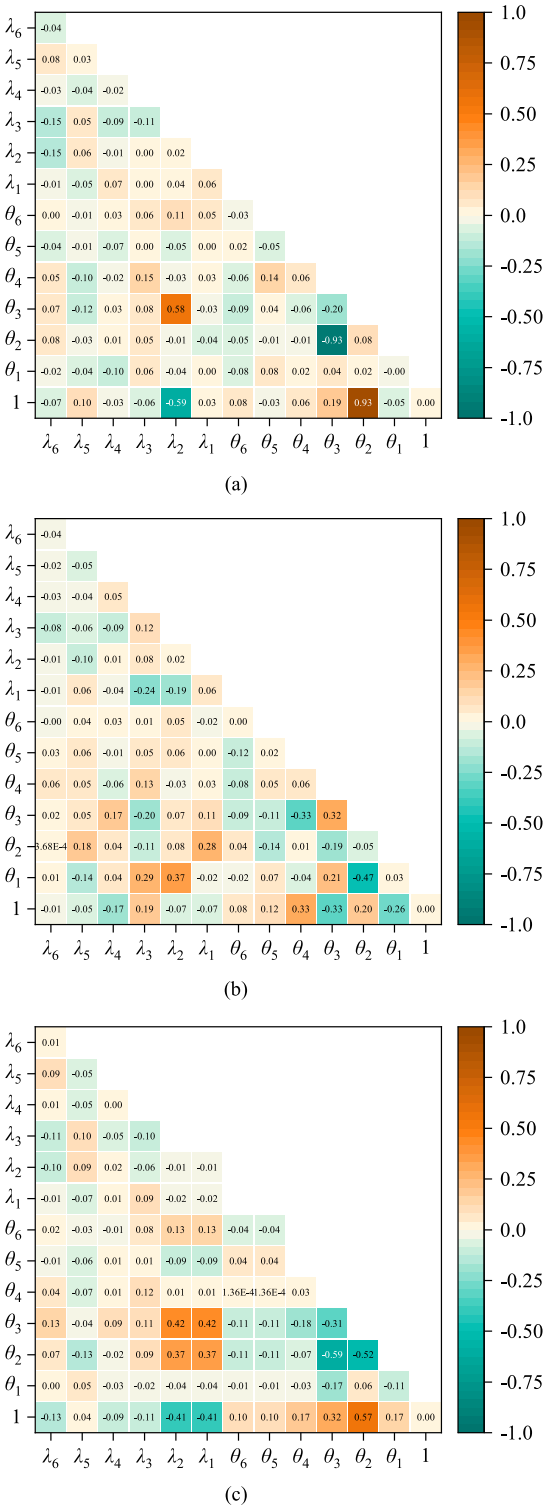

FIGURE 7. Pearson correlation matrix of candidate basis functions $[1, \theta_1, \theta_2, \cdots, \lambda_n, \theta_1^2, \cdots, \theta_1\lambda_n, \theta_2^2, \cdots, \lambda_n^2]_{1\times 91}$. (a) X_0 axis. (b),Y_0 axes. (c) Z_0 axis.

basis functions between the X_0, Y_0, and Z_0 axes indicate that the effect of the joint angle and rotation direction on the positioning error in each direction is distinct. And the basis functions with absolute correlation values greater than 0.1 for each axis, i.e., those with a correlation about positioning error,

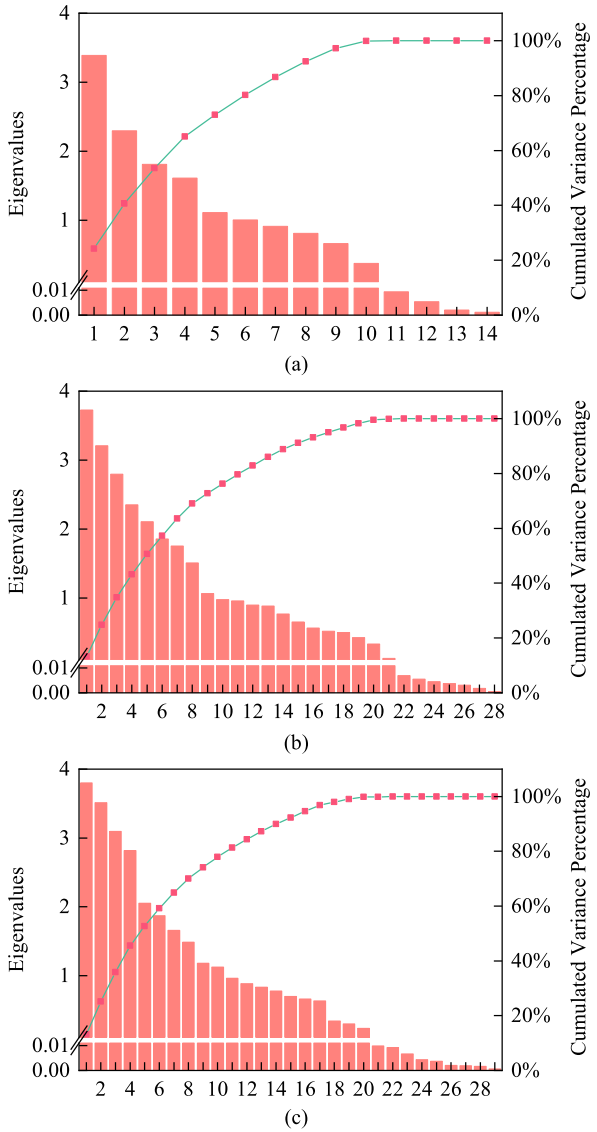

FIGURE 8. Dimension reduction through eigenvalue decomposition. (a) X_0 axis. (b) Y_0 axis. (c) Z_0 axis.

are chosen to compose the set of initial basis functions for further dimensionality reduction processing.

For the set of initial basis functions, PCA analysis was performed, and the variance and explained variance from PCA are depicted in Figure 8. It is obvious that the first few modified basis functions with high variances preserve the vast majority of the cumulative variances. Using the criterion of retaining more than 99% of the cumulative variance, the number of basis functions for the X_0, Y_0, and Z_0 axes has been reduced from 14, 28, 29 in the set of initial basis functions to 10, 20, 19 in the set of final basis functions, effectively reducing the complexity of basis functions.

2) ERROR MODEL FITTING

Four Kriging methods are utilized to model positioning errors for the X_0, Y_0, and Z_0 axes, respectively, and the accuracy of the surrogate models is compared quantitatively using

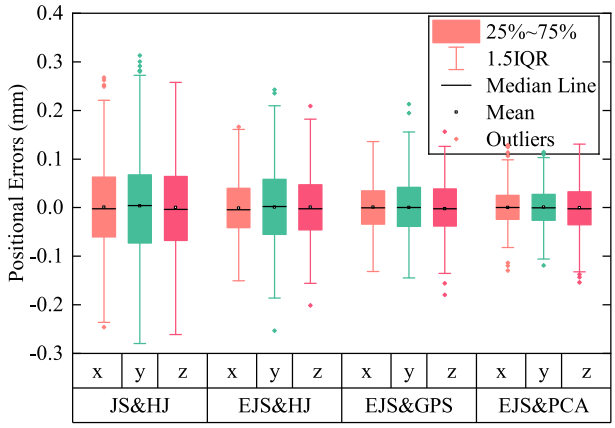

FIGURE 9. Box plots of estimation errors in the 10-fold cross-validation.

10-fold cross-validation. In the first method, JS&HJ, the HJ algorithm is used to determine the optimal correlation parameters in the joint space; in the second method, EJS&HJ, it takes a different strategy, that is, determining the optimal correlation parameters in the extended joint space; in the third method, EJS&GPS, the correlation coefficients ξ are optimized using the GPS algorithm in the extended joint space. In the fourth method, EJS&PCA, the dynamic Kriging method is introduced to optimize the basis function based on the EJS&GPS algorithm.

Figure 9 depicts box plots of estimation errors incurred by 10-fold cross-validation on 300 TCP error datasets using four Kriging algorithms. The results indicate that the EJS&PCA method obtained the best forecasting result compared to the other techniques. That is, the algorithm for dynamic Kriging was able to use the joint angle and directional coefficient information for better error estimation results. This is due to the fact that PCC and PCA effectively select the error-related basis functions while discarding the information overlap, which reduces the data dimensionality to prevent overfitting and improves the efficiency of the error model fitting, resulting in a more accurate surrogate model.

C. VERIFICATION OF THE ERROR COMPENSATION

After obtaining the surrogate model of the positioning error, 30 verification points in the robot's workspace are randomly chosen to validate the feasibility of the error feedforward compensation method. Using the error model and the feedforward compensation method proposed in Section III, validation point errors are compensated. Figure 10 shows the positioning errors of the verification points before and after position error compensation, and the statistical results are shown in Table 2.

The experimental results show that the maximum and average positioning errors of the robot are reduced by 0.3471 mm and 0.1856 mm, respectively, after Kriging interpolation in the robot's joint space and feedforward compensation, and further improve to 0.1848 mm and 0.1197 mm after adopting joint expanded space and dynamic

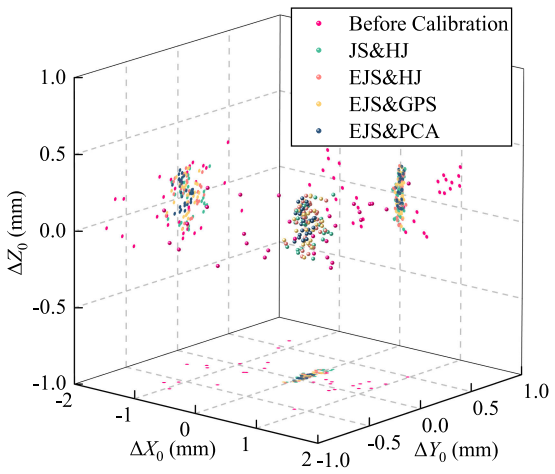

FIGURE 10. Comparison of positioning errors before compensation and after compensation.

TABLE 2. Statistical results of the positioning errors.

Method	Range (mm)	Mean(mm)	Standard Deviation (mm)
Before	[0.1456, 1.5157]	0.8562	0.3538
JS&HJ	[0.0428, 0.3471]	0.1856	0.0820
EJS&HJ	[0.0606, 0.2738]	0.1712	0.0588
EJS&GPS	[0.0465, 0.2514]	0.1531	0.0490
EJS&PCA	[0.0506, 0.1848]	0.1197	0.0326

Kriging interpolation, corresponding to reductions of 46.7% and 33.5%, respectively. This is due to the fact that the multi-directional repeatability error induced by the joint backlash is partially compensated, and the robot's positioning accuracy is enhanced.

V. CONCLUSION

A method for robot positioning error compensation based on the robot's extended joint space and the dynamic Kriging method is proposed. Beginning with the robot's kinematic model, the concept of extended joint space is proposed by introducing joint directional coefficients, and the spatial similarity of robot positioning errors in the extended joint space is then analyzed. Meanwhile, a new method called the dynamic Kriging method is proposed to fit the error model more accurately. In the dynamic Kriging method, an optimal basis function set is obtained using the basis functions that are selected and fusioned by PCC and PCA from the candidate basis functions, and GPS is used to find an accurate optimum for the correlation coefficient, and the positioning error is compensated by error feedforward compensation.

It can be seen from the experimental results that after Kriging interpolation in the robot joint space and feedforward compensation, the maximum/average positioning error of the robot improves from 1.5157 mm and 0.8562 mm before compensation to 0.3471 mm and 0.1856 mm after compensation, and further improves to 0.1848 mm and 0.1197 mm after adopting joint expansion space and dynamic Kriging method, which decreases by 46.7% and 33.5%, respectively. This method effectively compensates the multi-directional repeatability error introduced by the joint backlash and improves the robot's positioning precision. The method does not require the robot controller to be open, as it uses the spatial similarity of positioning errors in extended joint space for error modeling and compensates for positioning errors by adjusting the command point coordinates rather than the controller settings. The technology is simple to adopt in industrial applications because the robot is in open-loop control and no external measurement equipment is needed.

Further, to improve the robot's positioning accuracy under heavy loads, it is important to take into account the effect of load on the positioning error. This effect can be transformed into the effect of joint torque on the flexible joint angle. The calibration process is also upgraded to be integrated and software-based to form a fast, convenient, stable, and reliable system.

REFERENCES

[1] A. Gutierrez-Giles, L. U. Evangelista-Hernandez, M. A. Arteaga, C. A. Cruz-Villar, and A. Rodriguez-Angeles, "A force/motion control approach based on trajectory planning for industrial robots with closed control architecture," *IEEE Access*, vol. 9, pp. 80728–80740, 2021.

[2] Y. Zhang, K. Guo, J. Sun, and Y. Sun, "Method of postures selection for industrial robot joint stiffness identification," *IEEE Access*, vol. 9, pp. 62583–62592, 2021.

[3] J. Hu, F. Hua, and W. Tian, "Robot positioning error compensation method based on deep neural network," *J. Phys., Conf. Ser.*, vol. 1487, no. 1, Mar. 2020, Art. no. 012045.

[4] Y. Zeng, W. Tian, D. Li, X. He, and W. Liao, "An error-similarity-based robot positional accuracy improvement method for a robotic drilling and riveting system," *Int. J. Adv. Manuf. Technol.*, vol. 88, nos. 9–12, pp. 2745–2755, Feb. 2017.

[5] K. Guo, Y. Zhang, and J. Sun, "Towards stable milling: Principle and application of active contact robotic milling," *Int. J. Mach. Tools Manuf.*, vol. 182, Nov. 2022, Art. no. 103952.

[6] M. Pettersson and J. Ölvander, "Drive train optimization for industrial robots," *IEEE Trans. Robot.*, vol. 25, no. 6, pp. 1419–1424, Dec. 2009.

[7] A. Frommknecht, J. Kuehnle, I. Effenberger, and S. Pidan, "Multi-sensor measurement system for robotic drilling," *Robot. Comput. Integr. Manuf.*, vol. 47, pp. 4–10, Oct. 2017.

[8] P. Xiao, H. Ju, Q. Li, J. Meng, and F. Chen, "A new fixed axis-invariant based calibration approach to improve absolute positioning accuracy of manipulators," *IEEE Access*, vol. 8, pp. 134224–134232, 2020.

[9] G. Chen, T. Li, M. Chu, J. Xuan, and S. Xu, "Review on kinematics calibration technology of serial robots," *Int. J. Precis. Eng. Manuf.*, vol. 15, no. 8, pp. 1759–1774, Aug. 2014.

[10] T. Huang, D. Zhao, F. Yin, W. Tian, and D. G. Chetwynd, "Kinematic calibration of a 6-DOF hybrid robot by considering multicollinearity in the identification Jacobian," *Mechanism Mach. Theory*, vol. 131, pp. 371–384, Jan. 2019.

[11] V. Le Nguyen and R. J. Caverly, "Cable-driven parallel robot pose estimation using extended Kalman filtering with inertial payload measurements," *IEEE Robot. Autom. Lett.*, vol. 6, no. 2, pp. 3615–3622, Apr. 2021.

[12] G. Luo, L. Zou, Z. Wang, C. Lv, J. Ou, and Y. Huang, "A novel kinematic parameters calibration method for industrial robot based on Levenberg–Marquardt and differential evolution hybrid algorithm," *Robot. Comput.-Integr. Manuf.*, vol. 71, Oct. 2021, Art. no. 102165.

[13] S. Hayati and M. Mirmirani, "Improving the absolute positioning accuracy of robot manipulators," *J. Robot. Syst.*, vol. 2, no. 4, pp. 397–413, 1985.

[14] H. W. Stone and A. C. Sanderson, "A prototype arm signature identification system," in *Proc. IEEE Int. Conf. Robot.*, Apr. 1987, pp. 175–182.

[15] Y. Meng and H. Zhuang, "Autonomous robot calibration using vision technology," *Robot. Comput.-Integr. Manuf.*, vol. 23, no. 4, pp. 436–446, Aug. 2007.

[16] Y. Zhang, J. Cui, Y. Li, and Z. Chu, "Modeling and calibration of high-order joint-dependent kinematic errors of serial robot based on local POE," *Ind. Robot, Int. J. Robot. Res. Appl.*, vol. 50, no. 5, pp. 753–764, Aug. 2023.
[17] P.-N. Le and H.-J. Kang, "Robot manipulator calibration using a model based identification technique and a neural network with the teaching learning-based optimization," *IEEE Access*, vol. 8, pp. 105447–105454, 2020.
[18] W. Tian, M. Huo, X. Zhang, Y. Song, and L. Wang, "A general approach for robot pose error compensation based on an equivalent joint motion error model," *Measurement*, vol. 203, Nov. 2022, Art. no. 111952.
[19] W. Wang, W. Tian, W. Liao, B. Li, and J. Hu, "Error compensation of industrial robot based on deep belief network and error similarity," *Robot. Comput.-Integr. Manuf.*, vol. 73, Feb. 2022, Art. no. 102220.
[20] J. Qi, B. Chen, and D. Zhang, "A calibration method for enhancing robot accuracy through integration of kinematic model and spatial interpolation algorithm," *J. Mech. Robot*, vol. 13, no. 6, pp. 1–10, 2021.
[21] B. Li, W. Zhang, Y. Li, W. Tian, and C. Wang, "Positional accuracy improvement of an industrial robot using feedforward compensation and feedback control," *J. Dyn. Syst., Meas., Control*, vol. 144, no. 7, pp. 1–14, Jul. 2022.
[22] M. Slamani and I. A. Bonev, "Characterization and experimental evaluation of gear transmission errors in an industrial robot," *Ind. Robot, Int. J.*, vol. 40, no. 5, pp. 441–449, Aug. 2013.
[23] D. E. Whitney, C. A. Lozinski, and J. M. Rourke, "Industrial robot forward calibration method and results," *J. Dyn. Syst., Meas., Control*, vol. 108, no. 1, pp. 1–8, Mar. 1986.
[24] M. Cordes and W. Hintze, "Offline simulation of path deviation due to joint compliance and hysteresis for robot machining," *Int. J. Adv. Manuf. Technol.*, vol. 90, nos. 1–4, pp. 1075–1083, Apr. 2017.
[25] L. Ma, P. Bazzoli, P. M. Sammons, R. G. Landers, and D. A. Bristow, "Modeling and calibration of high-order joint-dependent kinematic errors for industrial robots," *Robot. Comput.-Integr. Manuf.*, vol. 50, pp. 153–167, Apr. 2018.
[26] D. A. Griffith and Y.-T. Liau, "Imputed spatial data: Cautions arising from response and covariate imputation measurement error," *Spatial Statist.*, vol. 42, Apr. 2021, Art. no. 100419.
[27] J. D. Martin and T. W. Simpson, "A study on the use of Kriging models to approximate deterministic computer models," in *Proc. Int. Design Eng. Tech. Conf. Comput. Inf. Eng. Conf.* Salt Lake City, UT, USA: ASME, Sep. 2003, p. 567.
[28] L. Zhao, K. K. Choi, and I. Lee, "Metamodeling method using dynamic Kriging for design optimization," *AIAA J.*, vol. 49, no. 9, pp. 2034–2046, Sep. 2011.
[29] B. Sparkman, J. Chrissis, M. Gruber, and M. Abramson, "Optimization of a scramjet fuel injection array: An application of mixed variable generalized pattern search with Kriging surrogates," in *Proc. 12th AIAA/ISSMO Multidisciplinary Anal. Optim. Conf.* Victoria, BC, Canada: AIAA, Sep. 2008, p. 5861.
[30] A. G. Asuero, A. Sayago, and A. González, "The correlation coefficient: An overview," *Crit. Rev. Anal. Chem.*, vol. 36, no. 1, pp. 41–59, 2006.
[31] R. Bro and A. K. Smilde, "Principal component analysis," *Anal. Methods*, vol. 6, no. 9, pp. 2812–2831, 2014.
[32] J. Camacho and A. Ferrer, "Cross-validation in PCA models with the element-wise k-fold (*ekf*) algorithm: Practical aspects," *Chemometric Intell. Lab. Syst.*, vol. 131, pp. 37–50, Feb. 2014.
[33] J. Santolaria and M. Ginés, "Uncertainty estimation in robot kinematic calibration," *Robot. Comput.-Integr. Manuf.*, vol. 29, no. 2, pp. 370–384, Apr. 2013.
[34] A. Nubiola and I. A. Bonev, "Absolute calibration of an ABB IRB 1600 robot using a laser tracker," *Robot. Comput.-Integr. Manuf.*, vol. 29, no. 1, pp. 236–245, Feb. 2013.

WEI HE received the B.S. degree in mechanical design and automation engineering and the M.S. degree in mechanical engineering from the Taiyuan University of Science and Technology, Taiyuan, China, in 2016 and 2019, respectively. He is currently pursuing the Ph.D. degree in mechanical engineering with Shandong University, Jinan, China.

His current research interests include inverse kinematics and motion planning for robots.

PIN ZHANG is currently a Senior Engineer with the AVIC Research Institute for Special Structures of Aeronautical Composites, Jinan, China. His current research interests include laser engraving, CNC machining, contemporary integrated manufacturing, flexible manufacturing, manufacturing execution systems, and automated manufacturing.

KAI GUO (Member, IEEE) received the Ph.D. degree in mechanical engineering from Zhejiang University, Hangzhou, China, in 2015.

He is currently an Assistant Professor with the Key Laboratory of High Efficiency and Clean Mechanical Manufacture of the Ministry of Education, Department of Mechanical Engineering, Shandong University, China. His current research interests include the design, modeling, and control of space robotics.

JIE SUN received the Ph.D. degree in mechanical engineering from Zhejiang University, Hangzhou, China, in 2004.

He is currently a Professor of mechanical engineering with Shandong University, Jinan, China. He has implemented several projects from the National Nature Science Foundation. He has authored or coauthored more than 100 journal articles. His current research interests include advanced design theory and manufacturing technology.

VINOTHKUMAR SIVALINGAM received the Ph.D. degree from the College of Engineering Guindy, Anna University, Chennai, India, in 2015.

He is currently an Associate Assistant Professor of mechanical engineering with Shandong University, Jinan, China. He has authored or coauthored more than 40 journals and conference papers. His current research interests include advanced machining processes and metrology and measurements.

XIAOMING HUANG received the Ph.D. degree in mechanical engineering from Shandong University, Jinan, China, in 2015.

He is currently an Associate Professor with the Mechatronics Engineering Department, Binzhou University, Binzhou, China. He has implemented several projects from the National Nature Science Foundation. His current research interest includes spacecraft design and fabrication.